Supramolecular block copolymers incorporating chiral and achiral chromophores for the bottom-up assembly of nanomaterials

Marta Riba-Moliner,[a] Cristina Oliveras-González,[b] David B. Amabilino[c] and Arántzazu González-Campo[a,*]

[a]*Institut de Ciència de Materials de Barcelona (ICMAB-CSIC), Campus Universitari, 08193 Bellaterra, Catalonia, Spain.*

[b]*Université d'Angers, CNRS Laboratoire MOLTECH-Anjou, UMR 6200, UFR Science, Bât. K, 2 Bd. Lavoisier, 49045 Angers, France.*

[c]*School of Chemistry, The University of Nottingham, University Park, Nottingham, NG7 2RD, UK*

Received date (to be automatically inserted after your manuscript is submitted)
Accepted date (to be automatically inserted after your manuscript is accepted)

ABSTRACT: The coordination of the chiral metalloporhyrin ([5,10,15,20-[4-(*R,R,R,R*)-2-N-octadecylamidoethyloxiphenyl] porphyrin] zinc (II)) and an achiral homologue to an amphiphilic block copolymer of poly(styrene-*b*-4-vinyl pyridine) (PS-*b*-P4VP) have been studied in solution and as cast material. The resulting chiral dye-polymer hybrid material has been accomplished via axial coordination between the zinc (II) metal ion in the core of the porphyrin ring and the pyridyl units of the block-copolymer in non-coordinative solvent. The supramolecular organisation and possible chirality transfer to the hybrid material have been studied in solution by UV-Visible absorption spectroscopy, fluorsecence spectroscopy, Nuclear Magnetic Ressonance and Circular Dichroism. The morphology of the chiral and achiral doped polymer has been studied in solid state by Transmission Electron Microscopy and Atomic Force Microscopy. We show that the nanostructures formed depend greatly upon the nature of the side chains on the porphyrins, where a chiral group leads to a very homogeneous phase separated material, perhaps indicating that chiral side groups are useful for the preparation of this type of supramolecular hybrid.

KEYWORDS: poly(styrene-*b*-4-vinyl pyridine) copolymer, chiral metalloporphyrin, doped film, micelles, hybrid material, axial coordination.

*Correspondence to: Arántzazu González-Campo, *Institut de Ciència de Materials de Barcelona (ICMAB-CSIC), Campus Universitari, 08193 Bellaterra, Catalonia, Spain, tel. +34 935801856, email: agonzalez@icmab.es*.

INTRODUCTION

Synthetic supramolecular chemistry has significant potential impact in the polymers field because the properties of the new hybrid materials are unique, thanks to their structures and functionalities [1]. For instance, polymer aggregation can be controlled by choosing recognition of strategic elements in macromolecular chains [2]. The aim of the present work is to combine these features with those of π-functional units. Porphyrins are versatile components in supramolecular systems [3-5], and they have been studied widely due to their optical and electronic properties, that make them suitable for a great variety of interests such as nanoelectronic systems [6], light-harvesting arrays [7] or dye-sensitizing chromophores in photovoltaic devices [8]. Their structural and physical properties are tuned by modifying either the side groups linked at the meso-position of the porphyrin ring or by chemical changes in the core, being the introduction of a metal ion in the chelating macrocycle the simplest modification possible [9, 10]. Free-base porphyrins and metalloporphyrins can self-assemble by non-covalent interactions [11] (such as hydrogen-bonding, π-π interactions or Van der Waals forces), but also the coordination of the metal ion with an exo-facing ligand can drive the self-assembly of the chromophores [12]. Recently, the ability of these metalloporphyrins to coordinate axial groups has led to a number of novel supramolecular constructs that may show interesting dynamic properties in the motion of the ring [13-15].

On the other hand, organic thin films based on amphiphilic block copolymers (BCPs) had been deeply studied due to the tunability of the different structural patterns adopted between the immiscible blocks at the interface [16-19]. The volume fraction of each block and the solvent used to dissolve/disperse them are the key factors to control the type of organisation adopted by the systems [20-24]. The BCP used here is poly(styrene-*b*-4-vinyl pyridine) (PS-*b*-P4VP), an amphiphilic macromolecule that contains well defined microstructures thanks to the incompatibility of the poly(styrene) (PS) and poly(4-vinyl pyridine) (P4VP) blocks with one another, its malleability, pH-responsiveness and the potential reactivity, and complex-forming ability of the P4VP block combined with the stiffness of the PS part. The P4VP block is selectively solubilised by polar protic solvents, except in water, in where it swells [25]. Conversely, the PS block is selectively soluble in non-polar solvents. There are some non-selective solvents that dissolve PS-*b*-P4VP completely, like chloroform and tetrahydrofuran and the corresponding polar-non-polar solvent mixtures. These 'solubility rules' depend on the molar fraction of each block and the degree of polymerization. Moreover, the amphiphilic character of the BCP allows a good phase separation that can be adjusted and, to some degree, induced by controlling the molar fraction and the solvent in which it is partially or totally solubilized. The variety of materials that can be achieved such as membranes, micelles and nanostructured thin films, among others with totally different final properties [26-30], and together with the use of the pyridine ring as an anchoring point have made this BCP applicable for a wide range of systems [31-33].

Here, the opportunities offered by the combination of PS-*b*-P4VP and a chiral zinc(II)-metalloporphyrin (Zn-(*R,R,R,R*)-**1**) are explored with the ultimate aim of obtaining dye-polymer hybrid materials via axial metal ion coordination for potential applications in optoelectronics [33, 34]. The zinc (II) metal ion located in the core of the porphyrin ring will provide the possibility of coordination by the pyridyl units of the BCP, resulting in supramolecular self-assembled systems [35]. For this purpose, chiral and achiral metalloporphyrins Zn-(*R,R,R,R*)-**1** and Zn-**2** were used (**Fig. 1**) [36-38]. The determination of the coordination between the PS-*b*-P4VP and the Zn-porphyrins, as well as the possible chirality transfer to the supramolecular organization of the BCP with the porphyrinic derivative compounds, will be studied in solution and in solid state by UV-Visible absorption spectroscopy (UV-Vis), Fluorescence spectroscopyand Circular Dichroism (CD) spectroscopy. Moreover, morphological studies of the superstructure formed

by the supramolecular hybrid will be analyzed by Transmission Electron Microscopy (TEM) and Atomic Force Microscopy (AFM).

<Fig. 1>

EXPERIMENTAL

General methods

Commercially available reagents and solvents. *S*tyrene ≥99%, 4-vinyl pyridine (containing 100 ppm hydroquinone as inhibitor), α-methystyrene 99% (containing 15 ppm p-tert-butylcatechol as inhibitor), the initiator sec-butyllithium (1.4 M in cyclohexane) and methanol (anhydrous, 99.8%) were purchased to Sigma-Aldrich. THF was HPLC degree from Teknokroma.

Measurements. UV-vis absorbance spectroscopy was mesuared using a Varian Cary 5000 UV-vis spectrophotometer, in solution with standardized quartz cuvettes of 1 cm of optical path were used. In solid experiments standardized quartz slides were used. Quartz surfaces were cleaned with piranha solution (H_2SO_4/H_2O_2 (30%); $3{:}1_{v/v}$) for 30 min prior their use. Nuclear Magnetic Resonance (NMR) spectra were recorded in a Bruker AVANCEII 300 and Bruker Avance DRX 300. Matrix-Assisted Laser Desorption-Ionization Mass Spectrometry (MALDI-TOF) measurements were performed with an Ultraflex (TOF/TOF) spectrometer. All Fourier Transform Infrared Spectroscopy (FTIR) measurements were recorded in Perkin Elmer (Spectrum one). The samples were of solid porphyrins (recovered after evaporation of solvent in a non-controlled precipitated way) and were performed in attenuated total reflection (ATR) mode. Porphyrins were measured on the plate of universal ATR (UATR). A Jasco J-275 spectropolarimeter was used for Circular Dichroism (CD) spectra measurements. A Peltier-temperature programmer for thermosetting the samples was used to cool the solutions. The samples were transferred to a standardized quartz cuvette to be analyzed. When the measured temperature was reached and stabilized, spectra were recorded. The Fluorescence spectroscopy measurements were performed using a Horiba-Jobin-Yvon SPEX Nanolog-TM and Cary eclipse spectrofluorimeters. All the samples were prepared, diluting a solid sample of the porphyrin and BCP in the corresponding amount of solvent. Transmission Electron Microscopy (TEM) images were acquired at 120 kV. TEM supports used were holey carbon coated copper grids (200 lines/inch). Only samples containing pure PS-*b*-P4VP were selectively stained with iodine vapors and the process was by placing the samples in a sealed container in iodine vapors atmosphere for 1 hour. 5 kV, a working distance of 10 mm, a spot of 3.5 and high vacuum were the conditions used to acquire Scanning Electron Microscopy (SEM) images. Energy-dispersive X-ray spectroscopy (EDAX) was assembled to SEM microscope, and to collect information 15 kV and analyzing times of ~2500 s were the fixed conditions.

Synthesis

Polymerization of PS-b-P4VP. PS-b-P4VP (molar ratio PS:P4VP 1:4) was synthesized following the methodology described by Varshney *et al.*[39]. The exact procedure, amounts and volumes employed in the reaction are detailed in the Supporting Information.

Synthesis of porphyrins Zn-(R,R,R,R)-1 and Zn-2. [5,10,15,20-[4-(R,R,R,R)-2-N-octadecylamidoethyloxiphenyl] porphyrin] zinc (II) (Zn-(R,R,R,R)-1) and [5,10,15,20-[4-N-octadecylacetamidophenoxy] porphyrin] zinc (II) (Zn-2) were prepared according to literature procedures [37][38].

Solid samples. A dome to reach vacuum conditions was used to obtain solid samples for TEM analyses of the phase segregation and micellar aggregation.

Polymeric doped micelles. Solvent exchange methodology: 3 mg of PS-b-P4VP and 0.25 mg of Zn-2 were dissolved in 1 mL of THF. Then, 4 mL of ultrapure water was added dropwise and THF was removed from the mixture by evaporation. In parallel, the inverse process, organic-to-selective organic solvent, was also tested by preparing a solution of 3 mg of PS-b-P4VP and 0.25 mg of Zn-2 in THF, adding 4 mL of 1,4-dioxane dropwise and removing the THF by simple evaporation. Both experiments (organic-to-selective polar and organic-to-selective organic solvents) were also performed with the chiral homologue Zn-(R,R,R,R)-1-based metallocompound.

RESULTS AND DISCUSSION

With the aim to corroborate the effectiveness of the coordination of a Zn-porphyrin with the pyridine units of the PS-*b*-P4VP (1:4), titration studies with the chiral metalloporphyrin Zn-(*R,R,R,R*)-**1** and the achiral Zn-**2** metalloporphyrin were conducted in solution using UV-Visible absorption spectroscopy [35]. Zinc (II) porphyrins tend to bind with nitrogen axial ligands, resulting in a red-shift of the absorption bands due to an increase of the electron density of the porphyrin ring [40, 41]. First, a titration study of the Zn-(*R,R,R,R*)-**1** with pyridine to form [Zn-(*R,R,R,R*)-**1**-(Py)] was followed by UV-Vis and used as a reference (**Fig. S1**). The titration was carried out at room temperature using a 5 μM solution in dichloromethane of the metalloporphyrin (Sol. A) and consecutive additions of a mixed solution (Sol. B) of pyridine (1.5 mM) and Zn-(*R,R,R,R*)-**1** (5 μM) in dichloromethane. After the addition of 0.15 mM of pyridine, a bathochromic shift of the Soret band from 423 nm to 430 nm was observed. The shift of the Q_α band was from 550 nm to 564 nm and, for the lower energy Q-band (Q_β) the shift was from 590 nm to 605 nm [40]. Moreover, the Q_β and showed a clear increase in the relative insensity with the increase of the pyridine amount. These results indicated the coordination of the pyridine with the Zinc (II) metal of the metalloporphyrin [41]. Towards the complexation BCP with the metalloporphyrins, a titration with the achiral Zn-**2** porphyrin was carried out at room temperature using a 50 μM solution of the metalloporphyrin (Sol. A) in chloroform. Concurrently, in order to avoid any dilution factor of the porphyrin respect of the BCP during the titration, a mixed solution composed by 47 μM of Zn-**2** and 0.5 mM of BCP in chloroform was prepared (Sol. B). The UV-Visible absorption analysis started with the measurement of the absorption of the metalloporphyrin solution (Sol. A) and continued with consecutive additions of Sol. B (**Fig. 2**). Additionally to the coordination between the pyridine groups of the BCP and the zinc (II) metal ion in the core of the porphyrin, Zn-**2** can self-assemble by the coordination of the carbonyl group of the amide in the periphery with the zinc of an adjacent metalloporphyrin [37]. However, the non-coordinating solvent and conditions used in the titration studies avoid the self-aggregation of the metalloporphyrin to study exclusively the effects of the coordination among porphyrins and the BCP [36].

<Fig. 2>

The UV-Visible absorption spectra of the titration showed the progressive and characteristic evolution of the Q-bands with the addition of BCP and the formation of the [Zn-**2**-(PS-*b*-P4VP)] complex (**Fig. 2**). Due to the concentrations used for the titration experiment, the signal of the Soret band was saturated and therefore, only the evolution of the Q-bands was followed. The absorption band corresponding to the Q_α band of the isolated Zn-**2** metallocompound (Sol. A) at 556 nm increased in intensity and shifted to 564 nm with the increase of the of PS-*b*-P4VP concentration. Similarly, the Q_β band experienced a bathochromic shift from 598 nm to 605 nm when the binding

to PS-*b*-P4VP occurred. The observed changes confirmed the axial coordination between the zinc (II) metal ion of the Zn-**2** and the nitrogen of the pyridine in solution, and therefore the formation of the [Zn-**2**-(PS-*b*-P4VP)] complex [35, 41]. The solution containing the complex was drop-cast on a quartz slide, and the film remaining after evaporation of the solvent was analyzed by UV-Visible absorption spectroscopy. The spectrum of the film showed a similar bathochromic shift of the Q_α and Q_β bands than the complex in solution (in both cases 11 nm) with respect to the pure Zn-**2** solution (**Fig. S2**). These results showed the viability of casting the complex for the preparation of films of [Zn-**2**-(PS-*b*-P4VP)].

The formation of the complex between the chiral metalloporphyrin Zn-(*R,R,R,R*)-**1** and the BCP was also proven both in solution and upon drop-casting onto quartz (**Fig. S3** and **Fig. S4**) by the red shift of the Q bands of the porphyrin. In solution, two isosbestic points appeared at 534 nm and at 588 nm in the UV-Visible absorption spectra (**Fig. S3**). As a film, the complex showed a similar absorption spectrum to the achiral complex (**Fig. S4**).

Fluorescence spectroscopic measurements of the metalloporphyrins and their complexes also confirmed the formation of the supramolecular polymer. The spectra of the chiral metalloporphyrin and its complex with the BCP showed emission from the first excited state (S_1) to the ground state (S_0) upon excitation at 551 nm and 601 nm for metalloporphyrin Zn-(*R,R,R,R*)-**1** and 554 nm and 601 nm for the complex [Zn-(*R,R,R,R*)-**1**-(PS-*b*-P4VP)], respectively (**Fig. 3**). The emission of the porphyrin in the complex was also red-shifted compared to the free compound. The Q_β-band presented a larger Stokes shift (62 nm) for the [Zn-(*R,R,R,R*)-**1**-(PS-*b*-P4VP)] complex than for the isolated metalloporphyrin Zn-(*R,R,R,R*)-1 (55 nm), due to the electron-donating character of the pyridyl group [42, 43].

<Fig. 3>

The chirality present in the side-chains of Zn-(*R,R,R,R*)-**1** could, in principle, lead to a chiral amplification, which could be observed through an increase of the optical activity of Zn-(*R,R,R,R*)-**1**-(PS-*b*-P4VP)] complex [12, 13, 44, 45]. Circular Dichroism (CD) spectroscopy is an extremely sensitivity probe for supramolecular structures [46]. Therefore, any proximity of porphyrin groups coordinated along the P4VP block should be detected using the technique. The complex was analyzed within the temperature range from 0 °C to 60 °C (**Fig. 4**). The CD spectra showed a slight temperature-dependece behaviour of the Zn-(*R,R,R,R*)-**1**-(PS-*b*-P4VP)] complex, being more evidence in the Q-bands in the corresponding absortion spectra. From 0°C to 20°C, clear CD signals were observed in the region of the Soret band and especially in the Q bands area. The intensity of these signals was very low (a few millidegrees), which is characteristic of chromophores in a chiral environment that is dominated by the stereochemistry point rather than chiral order between chromophores (which is, generally, much more intense) [47]. With the increase of the temperature, a significant decrease in the optical activity together with a slight blue-shift of the Q-bands absorption was observed, suggesting a possible de-coordination of the pyridyl units of the BCP and the zinc (II) metal ion of the porphyrin. On the other hand, CD studies of the film of the [Zn-(*R,R,R,R*)-**1**-(PS-*b*-P4VP)] complex on quartz gave only a noisy and low intensity CD signal response (**Fig. S5**). This result indicated that the transmission of chirality from the stereogenic centres to porphyrin organization was not effective in the complexes, where the average local achiral complex formation dominates. It should be pointed out that the pyridyl units can be in locally chiral positions, although the atactic nature of the polymer meant that a regular interaction between porphyrins coordinated to the same chain was not possible.

<Fig. 4>

In solution, ^{1}H NMR experiments were also performed consecutively to assess the binding between the metalloporphyrin and the BCP. Solutions of Zn-(*R,R,R,R*)-**1**, [Zn-(*R,R,R,R*)-**1**-(PS-*b*-P4VP)] complex and pure PS-*b*-P4VP in deuterated chloroform were studied at 298 K (**Fig. S6**). Some differences between the [Zn-(*R,R,R,R*)-**1**-(PS-*b*-P4VP)] complex and the PS-b-P4VP spectra were observed (**Fig. S6**). A slight shift and a broadening of the peaks positioned at 6.4 and 8.3 ppm were experienced after the coordination. These peaks correspond to the protons of pyridine groups of the BCP, whose changes were in concordance with the expected results [35][48]. Furthermore, the peak at 8.9 ppm for Zn-(*R,R,R,R*)-**1**, shifted down to 8.7 ppm when the porphyrin was coordinated, which correspond to the protons of the pyrrole rings.

Morphology of [Zn-2-(PS-b-P4VP)] and [Zn-(R,R,R,R)-1-(PS-b-P4VP)] complexes

The organization of the [Zn-**2**-(PS-*b*-P4VP)] and [Zn-(*R,R,R,R*)-**1**-(PS-*b*-P4VP)] complexes at the microscopic level as materials was studied by Atomic Force Microscopy (AFM) (see Supp. Info for sample preparation). The topography AFM images of [Zn-**2**-(PS-*b*-P4VP)] (**Fig. 5a-d**) and [Zn-(*R,R,R,R*)-**1**-(PS-*b*-P4VP)] (**Fig. 5e-h**) showed apparently quite different morphology at larger length scales (several microns). The achiral complex depicted a quite flat surface with apparent very thin flake-like features and larger solid particle-like features protruding from the surface (**Fig. 5a-d**). On the other hand, the complex incorporating the chiral porphyrin evidenced a very regular morphology, where flake-like objects (about 0.5 μm in width and 1-3 μm in length) are arranged randomly over the surface (**Fig. 5e-h**). Closer inspection of the surface (**Fig. 5f**) showed small round objects of approximately 20 nm high and 100 nm wide (**Fig. 5h**) localized between the flakes, which appeared rough but with no well-defined structure.

<Fig. 5>

These spotted features contrasted with the ones observed for the pure Zn-(*R,R,R,R*)-**1**, which arranged forming rounded dots-like (average diameter of 0.5 nm) (**Fig. S7**). This relevant difference in the packing highlighted the influence of incorporating the BCP in the self-assembly phenomenon of the complex. The morphology of the achiral complex exhibited similar nanometer scale round features, with the previously mentioned larger particles overlaid (**Fig. 5d**). These larger particles that appeared crystalline were presumably the small molecule (since they were not present in the other complex) and were dark in the phase image from the AFM (**Fig. 5c**). In this phase image, the higher flake-like regions also spotted dark, indicating that they corresponded to the porphyrin component, as well. In between these dark areas, quite well-defined nanostructured regions with dark dots were spotted, corresponding with the 20 nm-tall dots, in both the achiral and chiral samples. Therefore, the nanostructure of the material was similar in both cases, although more homogeneous in the case of the chiral porphyrin complex. These images contrasted with AFM images of pure PS-*b*-P4VP, prepared under same conditions (**Fig. S8**). The AFM topography of PS-*b*-P4VP (**Fig. S8a**) showed an irregular holed layer, probably as a consequence of the free evaporation of the solvent that created inhomogeneities during the evaporation and consequently, left locally dewetted regions. When the layer was analyzed closely, phase segregation from the continuous layer of the polymer was observed, although the holes were too large to obtain better contrasted images (**Fig. S8b**). As a consequence of the large holes, not much information could be extracted from the phase image (**Fig. S8c**). In summary, both, height profiles of the achiral and chiral metalloporphyrin-based complexes exhibited flake-like structures of ~ 35 nm in height and small spherical-shaped objects with averaged diameters of ~50 nm and ~100 nm in [Zn-**2**-(PS-*b*-P4VP)] and [Zn-(*R,R,R,R*)-**1**-(PS-*b*-P4VP)], respectively (**Fig. 5d** and **Fig. 5h**). Contrarily, the size of the objects observed in the pure polymer was ~10 nm (**Fig. S8d**).

Transmission Electron Microscopy (TEM) was used to determine the influence of the chirality of the metalloporphyrins in the phase segregation of the complexes. Separate solutions of PS-*b*-P4VP, [Zn-**2**-(PS-*b*-P4VP)] and [Zn-(*R,R,R,R*)-**1**-(PS-*b*-P4VP)] in chloroform were dried under vacuum for several hours until solid powders were afforded. The final powders were separately embedded in an epoxy resin and cured at 60°C for 2 days. Then, they were cut by using a microtome to finally obtain solid films with a thickness of 70-100 nm. The different samples were collected on holey-carbon copper TEM grids and were also selective stained with iodine vapours for 1 hour in a sealed container. TEM images of the pure block copolymer showed phase segregation with a quasi-lamellar structure, with darker domains corresponding to the P4VP block (as a consequence of the staining, used to enhance TEM contrast) (**Fig. 6a**). The [Zn-**2**-(PS-*b*-P4VP)] complex showed an unclear order (**Fig. 6b**). However, [Zn-(*R,R,R,R*)-**1**-(PS-*b*-P4VP)] chiral complex displayed very defined domains, dark areas with bright spots, probably arranging either in body-centered cubic spheres (fm3m), gyroid (ia3d) or inverse discontinuous cubic structure (fd3m) (**Fig. 6c**). These evidences, proved the effect of the presence of stereogenic centers in the alkyl chains of the porphyrin chains on the self-assembly of the supramolecular PS-*b*-P4VP complex, resulting in segregated regions with different structure. The chiral characteristic, given only by a single methyl group in each substituted alkyl chain, enlarged significantly the space domains between PS and P4VP, probably because of the higher steric hindrance between neighboring metalloporphyrin units anchored to the pyridyl groups.

<Fig. 6>

While the coordination of the porphyrin to the BCP in the composite material is clear, an alternative assembly strategy to obtain nanostructured materials was studied by modifying the polarity of solvents to obtain polymeric doped micelles [49-51]. Li and coworkers reported chiral core-shell micelles based on the electrostatic interactions between poly(ethylene glycol)-*b*-poly(4-vinyl pyridine) block copolymer and achiral free-based tetrakis(4-sulfonatophenyl) porphyrin [52]. Therefore, the complex formation using purely coordinative bonds in different solvents was explored. As starting point, 0.04 mM solutions of Zn-**2** and Zn-(*R,R,R,R*)-**1** and a dispersion (0.02 mM) of PS-*b*-P4VP in ethanol were prepared. Then, 1 mL of each solutions of Zn-**2** or Zn-(*R,R,R,R*)-**1** were mixed with 1 mL of PS-*b*-P4VP dispersion, respectively. Pure and mixed porphyrin-based solutions were drop-cast on carbon coated copper TEM grids for further analyses. The TEM measurements of Zn-**2** (**Fig. 7a**) revealed solid plate-like objects formed by the porphyrins, with approximate diameters of 650 nm. The coordination of Zn-**2** to PS-*b*-P4VP (**Fig. 7c**) resulted in an apparently porous network. In this unstained sample, the darker regions were presumably P4VP-Zn-**2**, similar to the observations of Yao *et al.* in aggregated chiral compound with achiral polymers [53]. On the other hand, TEM images of the chiral porphyrin Zn-(*R,R,R,R*)-**1** (**Fig. 7b**) evidenced a less dense material, even though some slice-like parts (less compact than the achiral porphyrin) were observed. More aggregated fibrous coiled elements were obtained than in Zn-**2**. In the [Zn-(*R,R,R,R*)-**1**-(PS-*b*-P4VP)] complex (**Fig. 7d**), well-defined 'cauliflower'-shaped structures were observed. A significantly more fibrous structure at the corona of the 'flowers' suggested that polymer coiled with Zn-(*R,R,R,R*)-**1**, leading twisted fibrous meshes.

<Fig. 7>

To further study the [Zn-(*R,R,R,R*)-**1**-(PS-*b*-P4VP)] complex morphology in ethanol, different preparation methodologies of the TEM samples were tested: (i) a drop of solution was cast on a holey-carbon copper TEM grid and directly analyzed, (ii) an aliquot of the solution was dried and then was embedded in an epoxy resin, the resin was cured

and then, cut using microtome in thin slices (70-100 nm) and analyzed by TEM without staining and, (iii) the same procedure as (ii) but the sample was stained with I_2 vapors for 1 hour in a sealed container before TEM imaging (**Fig. 8**). All the samples indicated similar superstructures, albeit with varying degrees of detail (**Fig. 8**). From the drop of the solution of the [Zn-(*R,R,R,R*)-**1**-(PS-*b*-P4VP)] complex analyzed directly by TEM (**Fig. 8a-b**) some regions with agglomerated matter and spherical aggregates with blurred perimeter were appreciated. The majority of the round objects were small but within a broad range of sizes (from 40 to 300 nm). The more continuous film seen in **Fig. 8a** indicated a twisted layer type structure. When the sample was prepared with epoxy resin, self-assembled Zn-(*R,R,R,R*)-**1** porphyrin domains became clearly visible in the continuous-type structure (**Fig. 8c**), and the aggregated particles were spotted, although no internal structure was evident (**Fig. 8d**). The dark regions in **Fig. 8c** probably corresponded to regions containing Zn-(*R,R,R,R*)-**1** porphyrin, forming stripes of 4 nm of separation, because the sample was not selectively stained. After enhancing the contrast by selectively staining the P4VP domains with I_2 vapours, the distribution of the BCP in the [Zn-(*R,R,R,R*)-**1**-(PS-*b*-P4VP)] micelles could be clearly appreciated as layers of ~4 nm of material (**Fig. 8e-f**). Images illustrated a possible twisted rope-like structure which could belong to P4VP domains, possibly coiled by the chiral effect of the porphyrin, although no handedness could be determined from the images.

<Fig. 8>

With the aim to elucidate if the self-assembled complex in the corona of micelles in ethanol, corresponding to the [Zn-(*R,R,R,R*)-**1**-(PS-*b*-P4VP)] complex, was optically active, CD measurements of the micelles in solution were performed (**Fig. S9**). However, no indication of chiral packing was observed, suggesting that no chiral chromophore interaction was present in the materials and, consequently, no significant chiral superstructure could be evidenced.

An alternative way to form the complex between the porphyrin and the BCP is by solvent exchange methodology [54, 55]. The solvent exchange procedure involves, firstly, dissolving the amphiphilic copolymer in a non-selective solvent and, secondly, adding slowly a selective solvent until the latter is in excess. Then, the non-selective solvent is removed (usually by evaporation), leading to a solvent exchange. In principle, progressive evaporation of the non-selective component induced the collapse of the solvophobic part of the copolymer, leading to a micelle-like structure (**Scheme 1**). To prove this, organic-to-selective polar solvent exchange was tested in the present systems

<Scheme 1>

PS-*b*-P4VP and the corresponding Zn-**2** or Zn-(*R,R,R,R*)-**1** porphyrin were dissolved in THF, ultrapure water was added dropwise and THF was removed from the mixture by evaporation. In parallel, the inverse process, organic-to-selective organic solvent, was also tested by the preparation of a solution of PS-*b*-P4VP and Zn-**2** or Zn-(*R,R,R,R*)-**1** in THF, addition of 1,4-dioxane dropwise and removal of the THF by simple evaporation. Additionally, control experiments for each solvent exchange process with pure PS-*b*-P4VP, Zn-**2** and Zn-(*R,R,R,R*)-**1** under same conditions and following the same procedures were performed. A drop of each final mixture was separately analyzed by TEM using holey-carbon copper grids. TEM images of PS-*b*-P4VP in water (**Fig. S10**) revealed well-defined round micelle-like objects with a narrow range of sizes (~150-400 nm). The P4VP phase was selectively stained with iodine vapors, appearing as dark regions. Klinger *et al.* observed similar micelles of PS-*b*-P2VP following a similar procedure [56]. When the solvent inducing the micellar assembly was 1,4-dioxane, a core of P4VP surrounded by a PS corona was expected [57]. TEM images of this sample showed smaller micellar structures than in water and surrounded by poorly

defined matter (blurry appearance) (**Fig. S11**). After staining, the P4VP domains appeared spherical (darker regions in the images) surrounded by the PS block, probably swollen as a result of the contact with 1,4-dioxane, and consequently, forming a blurred matter in their surroundings [58]. The volume fraction of the blocks in the PS-*b*-P4VP used here (molar ratio PS:P4VP of 1:4), surely determined sizes, distributions and behavior of micelle-like objects in the different solvents studied, due to the selectivity of each block. TEM image of pure Zn-**2** in water showed straight, planar and large ribbons morphologies (**Fig. S11a**) [59]. However, when 1,4-dioxane was used, Zn-**2** precipitated (**Fig. S11b**) forming mixed structures, plates (as observed from ethanol) as well as wider ribbons due to coordinative character of the solvent [60]. Moreover, TEM images of the chiral Zn-(*R,R,R,R*)-**1** precipitated in water (**Fig. S11c**) depicted very small round aggregates (sub-20 nm) with barely discernible fibrous sub-structure, being very different to the achiral homologue. When the solvent was 1,4-dioxane (**Fig. S11d**), similar aggregates to those in water were found, although with a larger surface (approximately 80 nm) with internal fibrous nanostructure.

On the other hand, TEM images of [Zn-**2**-(PS-*b*-P4VP)] formed very well-defined round and filled spheres (**Fig. 9a-d**). While in water and after the THF evaporation the spheres had a diameter of approximately 500 nm (**Fig. 9a-b**), from 1,4-dioxane mixture, the spheres had between 200 and 300 nm, with a rougher appearance (**Fig. 9c-d**). In both samples, darker spots were also seen inside the spheres, probably due to enriched porphyrin localized areas. For the sample prepared in water, in which the hydrophilic pyridyl fragments seems to be in contact with the water, unlike the organic solvent exchange, rougher and smaller particles with clear corona (presumably composed of PS domains) were observed (**Fig. 9a-b**). An increased tendency of aggregation between the particles in 1,4-dioxane was appreciated, due to the affinity between alkyl chains of neighboring packed porphyrins that could be swelled by the organic solvent (**Fig. 9c-d**).

<Fig. 9>

The chiral complex [Zn-(*R,R,R,R*)-**1**-(PS-*b*-P4VP)] also formed well defined particles in water, with approximately 500 nm in diameter (**Fig. 10a-b**), similar to its achiral homologue. Contrarily, when the chiral metallocompound was immersed in 1,4-dioxane (**Fig. 10c-d**), no particulate aggregation was observed, only polymer phase segregation and aggregates could be discerned (**Fig. 10c**). Apparently, no coordination between the PS-*b*-P4VP and Zn-(*R,R,R,R*)-**1** was concluded, and coordination of the zinc (II) with the 1,4-dioxane occurred [60]. This fact was assumed because of the higher solubility of the chiral porphyrin in contrast to the achiral one, and the large excess of solvent used compared to the polymer amount. Snitka and coworkers observed similar striped structures (they designated them molecular ribbons) in aggregates of tetrakis(4-sulfonatophenyl)porphyrin, supporting the coordination of the precursors by the solvent [61].

<Fig. 10>

CONCLUSIONS

The binding of both achiral and chiral zinc (II) porphyrins to the pyridyl block of the polymer is clear both in solution in a non-coordinating solvent (chloroform) and in films. The system can also be used to make nanomaterials whose morphology depends on the chiral or non-chiral form of the coordinated zinc (II) porphyrin analogue. The coordinated systems [Zn-2-(PS-b-P4VP)] and [Zn-(R,R,R,R)-1-(PS-b-P4VP)] have differences in their morphology as cast materials, observing more uniformity for the chiral complex, as well as when precipitation under far-from-

equilibrium conditions occurred. Notably, the precipitation in water generates the most homogeneous material although no well-defined substructure exists in the particle generated. The chiral complex does not show significant optical activity, either in solution or in the nanomaterials prepared, indicating that the polymer coordination prevents the proximity of the chromophores and stereogenic centres. This situation contrasts dramatically from the one in which the pure porphyrins stack on top of one another thanks to hydrogen bonding, leading to significant optical activity. It also indicates that this kind of polymer with an atactic and rigid structure in combination with the necessary axial coordination of the pyridine groups and the chiral zinc (II) porphyrins is not suited. Therefore, a block copolymer with a control of the tacticity and phase segregation will be more appropriate for further studies of chirality transfer in this kind of dye-polymer hybrid material.

Acknowledgements

We thank T. Parella (UAB) for its help in DOSY-NMR measurements, J. Oró (ICMAB) for its help in TEM imaging and M. Simón (ICMAB) for its help in AFM imaging. The work was supported by MINECO with the Project MAT2016-77852-C2-1-R (AEI/FEDER, UE) and MAT2013-47869-C4-2-P and Generalitat de Catalunya for the project 2017-SGR-1277. AGC acknowledges financial support from the Spanish Ministry of Economy and Competitiveness, through the "Severo Ochoa" Programme for Centres of Excellence in R&D (SEV- 2015-0496) and the Ministry of Science, Innovation and Universities for a Ramon y Cajal contract (RYC-2017-22910).

REFERENCES

1. Harada A. *Supramolecular Polymer Chemistry*, Wiley-VCH Verlag GmbH & Co. KGaA, 2011.
2. Thibault RJ, Rotello VM. *Molecular Recognition and Polymers*, John Wiley & Sons, Inc., 2008; 1-7.
3. Elemans JAAW, Van Hameren R, Nolte RJM, Rowan AE. *Adv. Mater.* 2006; **18**: 1251-1266.
4. Yan Q, Luo Z, Cai K, Ma Y, Zhao D. *Chem. Soc. Rev.* 2014; **43**: 4199-4221.
5. Zhang C, Chen P, Dong H, Zhen Y, Liu M, Hu W. *Adv. Mater.* 2015; **27**: 5379-5387.
6. Aragonès AC, Darwish N, Saletra WJ, Pérez-García L, Sanz F, Puigmartí-Luis J, Amabilino DB, Díez-Pérez I. *Nano Lett.* 2014; **14**: 4751-4756.
7. Imahori H. *J. Phys. Chem. B*. 2004; **108**: 6130-6143.
8. Louahem M'Sabah B, Boucharef M, Warnan J, Pellegrin Y, Blart E, Lucas B, Odobel F, Boucle J. *Phys. Chem. Chem. Phys.* 2015; **17**: 9910-9918.
9. Goldberg I. *Chem. Comm.* 2005; **10**: 1243-1254.
10. Chmielewski PJ, Latos-Grażyński L. *Coord. Chem. Rev.* 2005; **249**: 2510-2533.
11. Pasternack RF, Giannetto A, Pagano P, Gibbs EJ. *J. Am. Chem. Soc.* 1991; **113**: 7799-7800.
12. Beletskaya I, Tyurin VS, Tsivadze AY, Guilard R, Stern C. *Chem. Rev.* 2009; **109**: 1659-1713.
13. Ogi S, Ikeda T, Wakabayashi R, Shinkai S, Takeuchi M. *Chem. Eur. J.* 2010; **16**: 8285-8290.
14. Sguerra F, Bulach V, Hosseini MW. *Dalton Trans.* 2012; **41**: 14683-14689.
15. Puigmarti-Luis J, Saletra WJ, Gonzalez A, Amabilino DB, Pérez-García L. *Chem. Comm.* 2014; **50**: 82-84.
16. Hamley IW. *Prog. Polym. Sci.* 2009; **34**: 1161-1210.
17. Kim JK, Yang SY, Lee Y, Kim Y. *Prog. Polym. Sci.* 2010; **35**: 1325-1349.
18. Heier J, Kramer EJ, Walheim S, Krausch G. *Macromolecules* 1997; **30**: 6610-6614.
19. Albert JNL, Epps III TH. *Mater. Today* 2010; **13**: 24-33.
20. Bates FS, Fredrickson GH. *Phys. Today* 1999; **52**: 32-38.
21. Gowd EB, Böhme M, Stamm M. *IOP C. Ser. Mater. Sci. En.* 2010; **14**: 012015.
22. Sinturel C, Vayer M, Morris M, Hillmyer MA. *Macromolecules* 2013; **46**: 5399-5415.

23. Kao J, Thorkelsson K, Bai P, Rancatore BJ, Xu T. *Chem. Soc. Rev.* 2013; **42**: 2654-2678.
24. Gowd EB, Koga T, Endoh MK, Kumar K, Stamm M. *Soft Matter.* 2014; **10**: 7753-7761.
25. D'Aprano A, Fuoss RM. *J. Polym. Sci.* 1969; **7**: 1101-1109.
26. Letchford K, Burt H. *Eur. J. Pharm. Biopharm.* 2007; **65**: 259-269.
27. Li X, Han Y. *J. Mater. Chem.* 2011; **21**: 18024-18033.
28. Radjabian M, Koll J, Buhr K, Handge UA, Abetz V. *Polymer* 2013; **54**: 1803-1812.
29. Clodt JI, Filiz V, Rangou S, Buhr K, Abetz C, Höche D, Hahn J, Jung A, Abetz V. *Adv. Func. Mater.* 2013; **23**: 731-738.
30. Klinger D, Wang CX, Connal LA, Audus DJ, Jang SG, Kraemer S, Killops KL, Fredrickson GH, Kramer EJ, Hawker CJ. *Angew. Chem. Int. Ed.* 2014; **53**: 7018-7022.
31. Bronstein LM, Sidorov SN, Valetsky PM, Hartmann J, Cölfen H, Antonietti M. *Langmuir* 1999; **15**: 6256-6262.
32. Guldi DM, Rahman GM, Qin S, Tchoul M, Ford WT, Marcaccio M, Paolucci D, Paolucci F, Campidelli S, Prato M. *Chem. Eur. J.* 2006; **12**: 2152-2161.
33. Arulkashmir A, Mahale RY, Dharmapurikar SS, Jangid MK, Krishnamoorthy K. *Polym. Chem.* 2012; **3**: 1641-1646.
34. Huang HX, Liu J, Cai YQ. *J. Lumin.* 2013; **143**: 447-452.
35. Gao B, Wang R, Du R. *J. Porphyr. Phthalocya.* 2010; **14**: 235-243
36. Oliveras-González C, Di Meo F, González-Campo A, Beljonne D, Norman P, Simón-Sorbed M, Linares M, Amabilino, DB. *J. Am. Chem. Soc.* 2015; **137**: 15795-15808.
37. Feldborg LN, Saletra WJ, Iavicoli P, Amabilino DB. *J. Porphyr. Phthalocya.* 2011; **15**: 995-1003.
38. Iavicoli P, Xu H, Feldborg LN, Linares M, Paradinas M, Stafström S, Ocal C, Nieto-Ortega B, Casado J, López Navarrete JT, Lazzaroni R, Feyter SD, Amabilino DB. *J. Am. Chem. Soc.* 2010; **132**: 9350-9362.
39. Varshney SK, Zhong XF, Eisenberg A. *Macromolecules* 1993; **26**: 701-706
40. Gautam R, Chauhan SMS. *Mater. Sci. Eng. C Mater.* 2014; **43**: 447-457.
41. Alessio E. *Structure and bonds: Non-covalent multi-porphyrin assemblies: synthesis and properties*, Springer, 2006; **121**, 1-47.
42. Apanasovich VV, Novikov EG, Yatskov NN, Koehorst RBM, Schaafsma TJ, van Hoek A. *J. Appl. Spectrosc.* 1999; **66**: 613-616.
43. Karolczak J. Kowalska D, Lukaszewicz A, Maciejewski A, Steer RP. *J. Phys. Chem. A* 2004; **108**: 4570-4575.
44. Green MM, Reidy MP, Johnson RD, Darling G, O'Leary DJ, Willson G. *J. Am. Chem. Soc.* 1989; **111**: 6452-6454.
45. Palmans ARA, Meijer EW. *Angew.Chem. Int. Ed.* 2007; **46**: 8948-8968.
46. Gottarelli G, Lena S, Masiero S, Pieraccini S, Spada GP. *Chirality* 2008; **20**: 471-485.
47. Pescitelli G, Di Bari L, Berova N. *Chem. Soc. Rev.* 2014; **43**: 5211-5233.
48. Pale V, Nikkonen T, Vapaavuori J, Kostianien M, Kavakka J, Selin J, Tittonen I, Helaja J. *J. Mater. Chem. C* 2013; **1**: 2166-2173.
49. Štěpánek M, Matějíček P, Humpolíčková J, Havránková J, Podhájecká K, Špírková M, Tuzar Z, Tsitsilianis C, Procházka K. *Polymer* 2005; **46**: 10493-10505.
50. Fan H, Jin Z, *Soft Matter* 2014; **10**: 2848-2855.
51. Connal LA, Lynd NA, Robb MJ, See KA, Jang SG, Spruell JM, Hawker CJ. *Chem. Mater.* 2012; **24**: 4036-4042.
52. Li J, An Y, Chen X, Xiong DA, Li Y, Huang N, Shi L. *Macromol. Rapid Commun.* 2008; **29**: 214-218.
53. Yao L, Lu X, Chen S, Watkins JJ. *Macromolecules* 2014; **47**: 6547-6553.
54. Robb MJ, Connal LA, Lee BF, Lynd NA, Hawker CJ. *Polym. Chem.* 2012; **3**: 1618-1628.
55. Krogstad DV, Lynd NA, Choi SH, Spruell JM, Hawker CJ, Kramer EJ, Tirrell MV. *Macromolecules* 2013; **46**: 1512-1518.
56. Klinger D, Robb MJ, Spruell JM, Lynd NA, Hawker CJ, Connal LA. *Polym. Chem.* 2013; **4**: 5038-5042.

57. Bharatiya B, Schumers JM, Poggi E, Gohy JF. *Polymers* 2013; **5**: 679-695.
58. Nunes SP, Karunakaran M, Pradeep N, Behzad AR, Hooghan B, Sougrat R, He H, Peinemann KV, *Langmuir* 2011; **27**: 10184-10190.
59. Ogi S, Sugiyasu K, Manna S, Samitsu S, Takeuchi M. *Nat. Chem.* 2014; **6**: 188-195.
60. Mikhalitsyna EA, Tyurin VS, Nefedov SE, Syrbu SA, Semeikin AS, Koifman OI, Beletskaya IP. *Eur. J. Inorg. Chem.* 2012; **12**: 5979-5990.
61. Snitka V, Rackaitis M, Rodaite R. *Sensor. Actuat. B-Chem.* 2005; **109:** 159-166

FIGURES AND SCHEME CAPTIONS

Fig. 1. Representation of the coordination of the Zn-porphyrins and the PS-*b*-P4VP after their axial coordination

Fig. 2. UV-Visible absorption spectra of the titration between Zn-2 (Sol. A) and Zn-2/PS-b-P4VP (Sol. B) to form the [Zn-2-(PS-b-P4VP)] complex in chloroform

Fig. 3. UV-Visible absorption and fluorescence spectra of Zn-(*R,R,R,R*)-**1** (5 μM) and [Zn-(*R,R,R,R*)-**1**-(PS-*b*-P4VP)] complex (5 μM) in chloroform solution.

Fig. 4. CD and corresponding and the corresponding absorption spectra of [Zn-(*R,R,R,R*)-**1**-(PS-*b*-P4VP)] complex in chloroform solution (50 μM) within the temperature range 0°C to 60 °C. HT(V) means Hight Tension (Voltage)

Fig. 5. AFM images of [Zn-**2**-(PS-*b*-P4VP) (a-d) and [Zn(*R,R,R,R*)-**1**-(PS-*b*-P4VP)] (e-h) coordinated compounds from a solution of chloroform drop-casted on HOPG surfaces. Topography images are shown in a and e (scale bars indicate 5 μm), b and f are closer-up topographic images from a and e (indicated with red dashed lines) (blue dashed lines indicate where the height profiles were taken from) (scale bars indicate 1 μm) and c and g are phase images corresponding to topographic images b and f (scale bars indicate 1 μm). Height profiles corresponding to the horizontal dashed lines in b, f are shown in d and h

Fig. 6. TEM images of a) the pure PS-*b*-P4VP, and the porphyrin complexes b) [Zn-**2**-(PS-*b*-P4VP)] and c) [Zn-(*R,R,R,R*)-**1**-(PS-*b*-P4VP)], obtained by microtoming solid samples from a dried chloroform solution. (Scale bars indicate 100 nm)

Fig. 7. TEM images of Zn-porphyrins and their complexes with PS-*b*-P4VP obtained from solutions in ethanol by drop-casting on carbon coated copper a) Zn-**2** (scale bar indicates 100 nm), b) Zn-(*R,R,R,R*)-**1** (scale bar indicates 100 nm), c) [Zn-**2**-(PS-*b*-P4VP)] (scale bar indicates 200 nm), d) [Zn-(*R,R,R,R*)-**1**-(PS-*b*-P4VP)] (scale bar indicates 50 nm).

Fig. 8. TEM images of [Zn-(*R,R,R,R*)-**1**-(PS-*b*-P4VP)] samples prepared from ethanol. a) and b) from a drop of the mixed solution without staining, c) and d) from the dried mixed solution embedded in an epoxy resin without staining and, e) and f) from dried mixed solution embedded in an epoxy resin stained with I_2 vapours. (Scale bars indicate 20 nm)

Fig. 9. Pictures of [Zn-**2**-(PS-*b*-P4VP)] solutions in water (greenish) and in 1,4-dioxane (pale rose). TEM images of [Zn-**2**-(PS-*b*-P4VP)] micelles in water a) and b) and, in 1,4-dioxane c) and d). (a and c scale bars indicate 100 nm; b and d scale bars indicate 50 nm)

Fig. 10. Pictures of [Zn-(*R,R,R,R*)-**1**-(PS-*b*-P4VP)] solutions in water (greenish) and 1,4-dioxane (pink) and TEM images of: a) and b) [Zn-(*R,R,R,R*)-**1**-(PS-*b*-P4VP)] micelles in water and, c) and d) [Zn-(*R,R,R,R*)-**1**-(PS-*b*-P4VP)] mixed compound in 1,4-dioxane. (a scale bar indicates 100 nm; b scale bar indicates 50 nm; c scale bar indicates 200 nm; d scale bar indicates 50 nm)

Scheme 1. Representation of the formation of the PS-*b*-P4VP micelles depending on the polarity of the solvent (solvent exchange method)

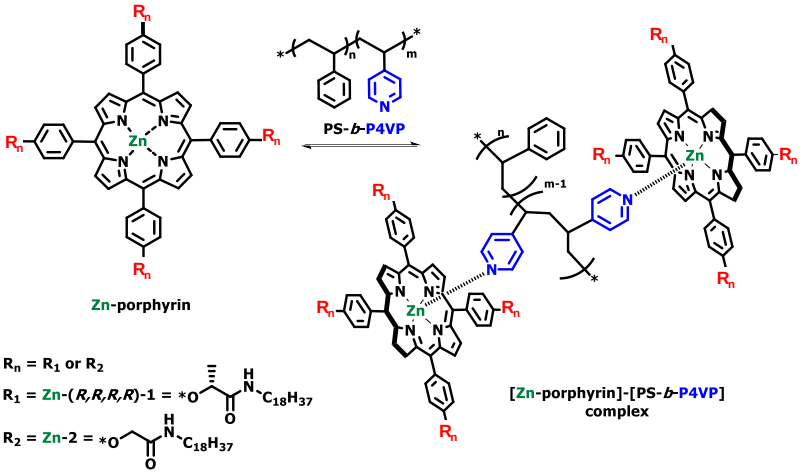

Fig. 1. Representation of the coordination of the Zn-porphyrins and the PS-*b*-P4VP after their axial coordination

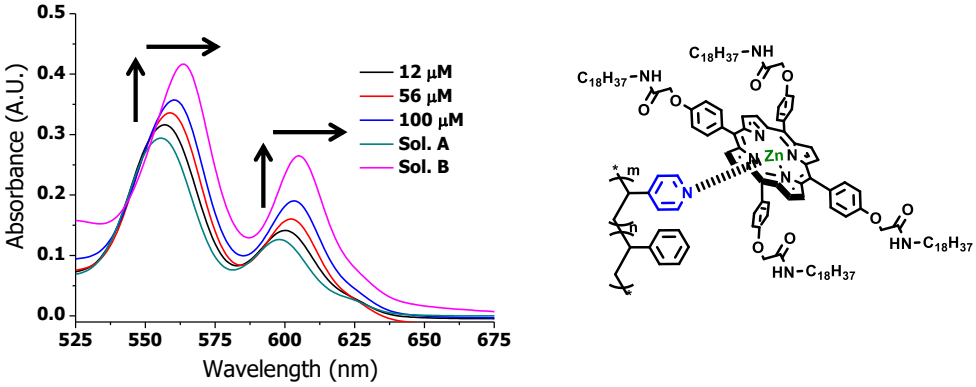

Fig. 2. UV-Visible absorption spectra of the titration between Zn-2 (Sol. A) and Zn-2/PS-b-P4VP (Sol. B) to form the [Zn-2-(PS-b-P4VP)] complex in chloroform.

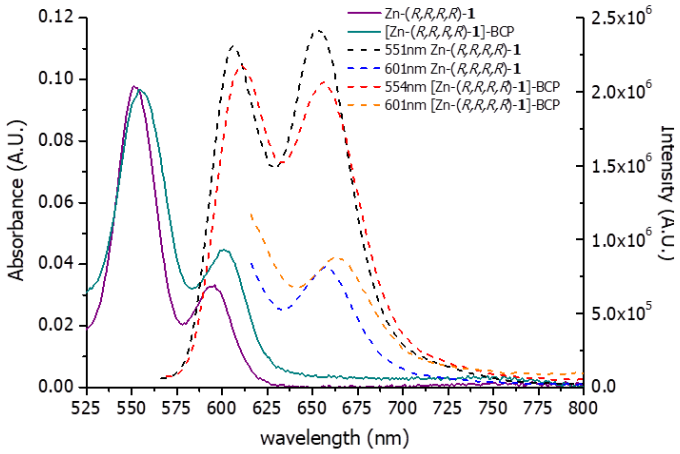

Fig. 3. UV-Visible absorption and fluorescence spectra of Zn-(*R,R,R,R*)-**1** (5 μM) and [Zn-(*R,R,R,R*)-**1**-(PS-*b*-P4VP)] complex (5 μM) in chloroform solution.

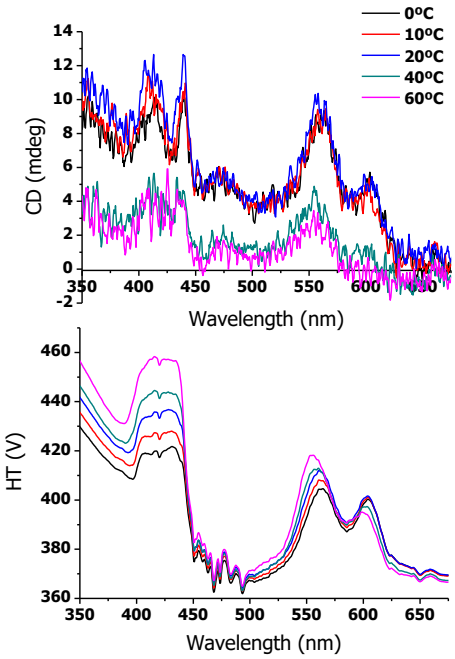

Fig. 4. CD and corresponding and the corresponding absorption spectra of [Zn-(*R,R,R,R*)-**1**-(PS-*b*-P4VP)] complex in chloroform solution (50 μM) within the temperature range 0ºC to 60 ºC. HT(V) means Hight Tension (Voltage)

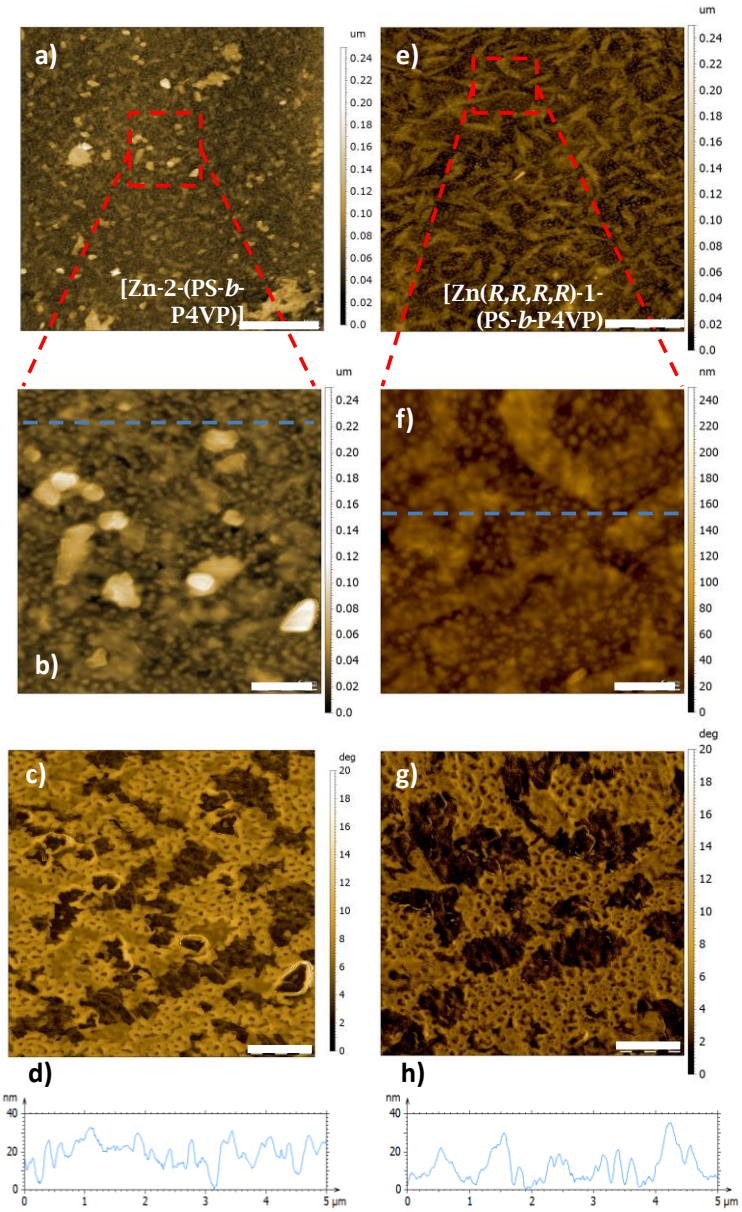

Fig. 5. AFM images of [Zn-**2**-(PS-*b*-P4VP) (a-d) and [Zn(*R,R,R,R*)-**1**-(PS-*b*-P4VP)] (e-h) coordinated compounds from a solution of chloroform drop-casted on HOPG surfaces. Topography images are shown in a and e (scale bars indicate 5 µm), b and f are closer-up topographic images from a and e (indicated with red dashed lines) (blue dashed lines indicate where the height profiles were taken from) (scale bars indicate 1 µm) and c and g are phase images corresponding to topographic images b and f (scale bars indicate 1 µm). Height profiles corresponding to the horizontal dashed lines in b, f are shown in d and h.

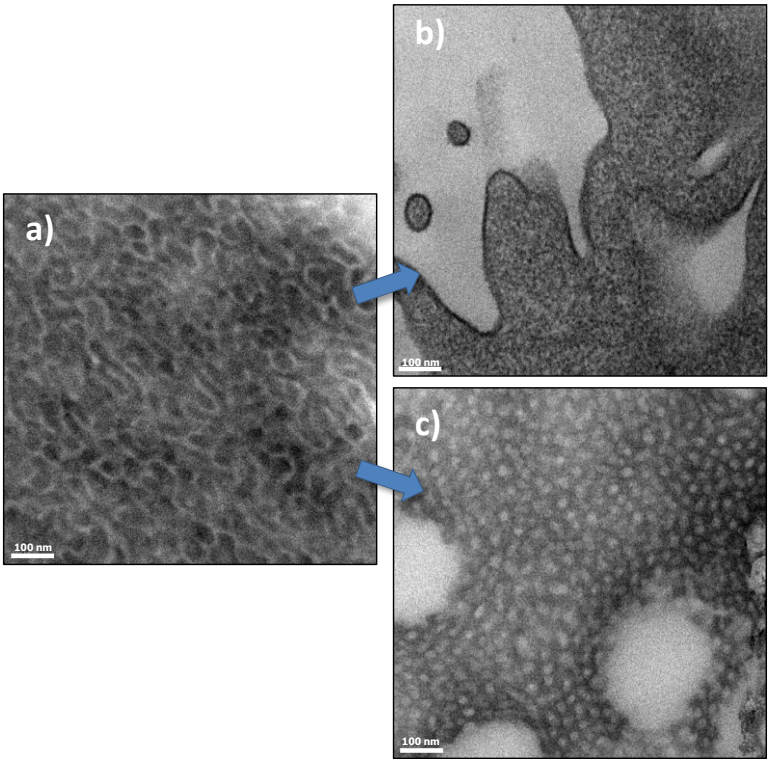

Fig. 6. TEM images of a) the pure PS-*b*-P4VP, and the porphyrin complexes b) [Zn-**2**-(PS-*b*-P4VP)] and c) [Zn-(*R,R,R,R*)-**1**-(PS-*b*-P4VP)], obtained by microtoming solid samples from a dried chloroform solution. (Scale bars indicate 100 nm)

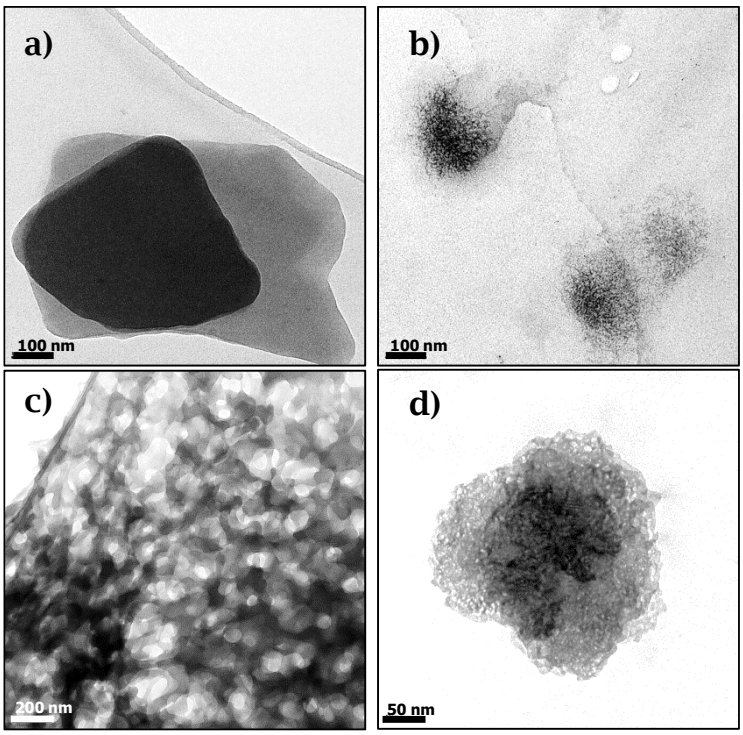

Fig. 7. TEM images of Zn-porphyrins and their complexes with PS-*b*-P4VP obtained from solutions in ethanol by drop-casting on carbon coated copper a) Zn-**2** (scale bar indicates 100 nm), b) Zn-(*R,R,R,R*)-**1** (scale bar indicates 100 nm), c) [Zn-**2**-(PS-*b*-P4VP)] (scale bar indicates 200 nm), d) [Zn-(*R,R,R,R*)-**1**-(PS-*b*-P4VP)] (scale bar indicates 50 nm).

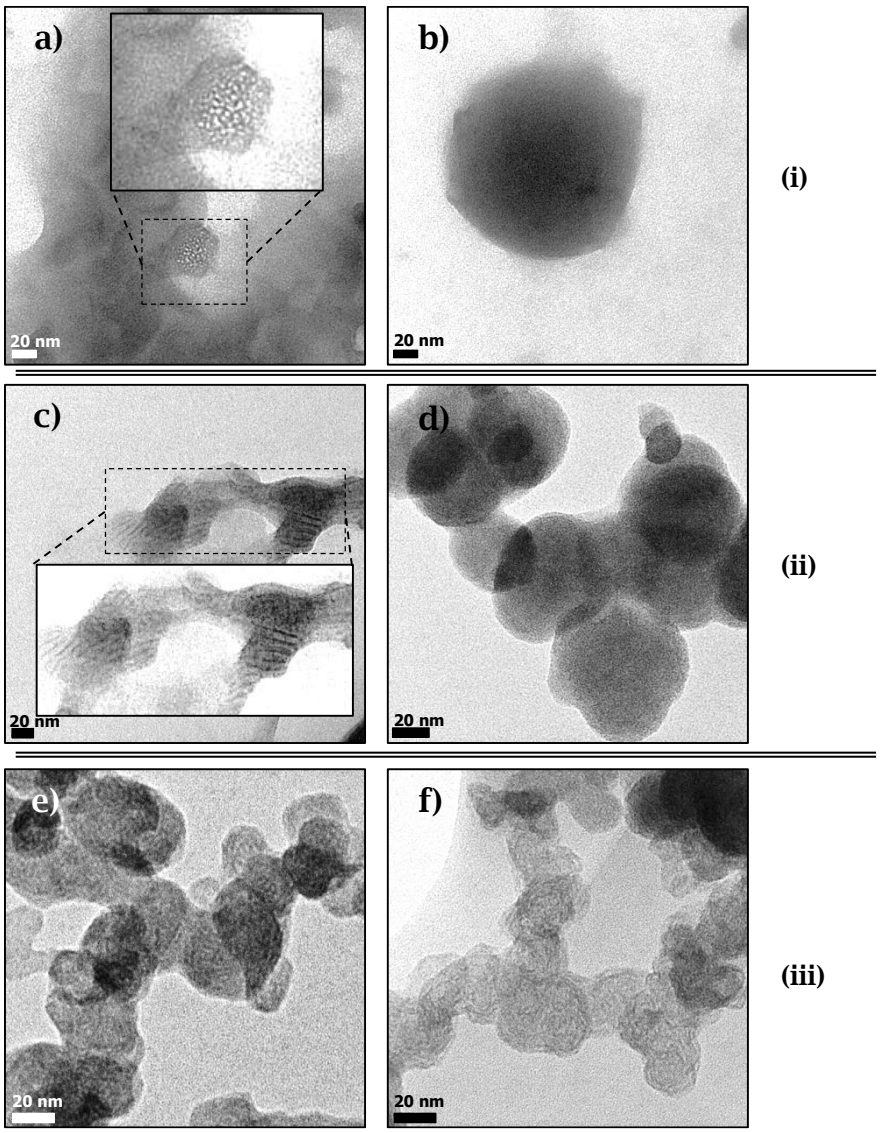

Fig. 8. TEM images of [Zn-(*R,R,R,R*)-**1**-(PS-*b*-P4VP)] samples prepared from ethanol. a) and b) from a drop of the mixed solution without staining, c) and d) from the dried mixed solution embedded in an epoxy resin without staining and, e) and f) from dried mixed solution embedded in an epoxy resin stained with I_2 vapours. (Scale bars indicate 20 nm)

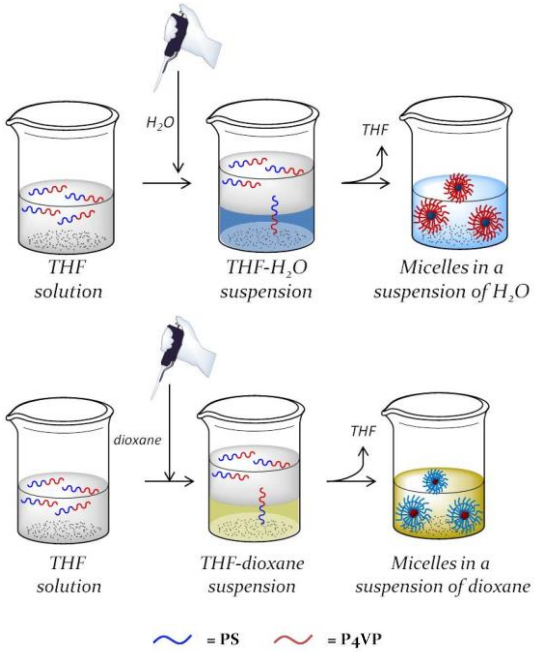

Scheme 1. Representation of the formation of the PS-*b*-P4VP micelles depending on the polarity of the solvent (solvent exchange method)

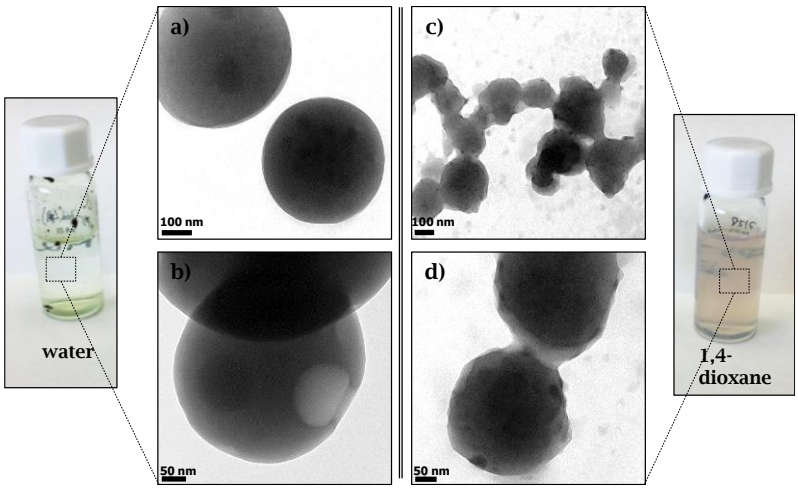

Fig. 9. Pictures of [Zn-**2**-(PS-*b*-P4VP)] solutions in water (greenish) and in 1,4-dioxane (pale rose). TEM images of [Zn-**2**-(PS-*b*-P4VP)] micelles in water a) and b) and, in 1,4-dioxane c) and d). (a and c scale bars indicate 100 nm; b and d scale bars indicate 50 nm)

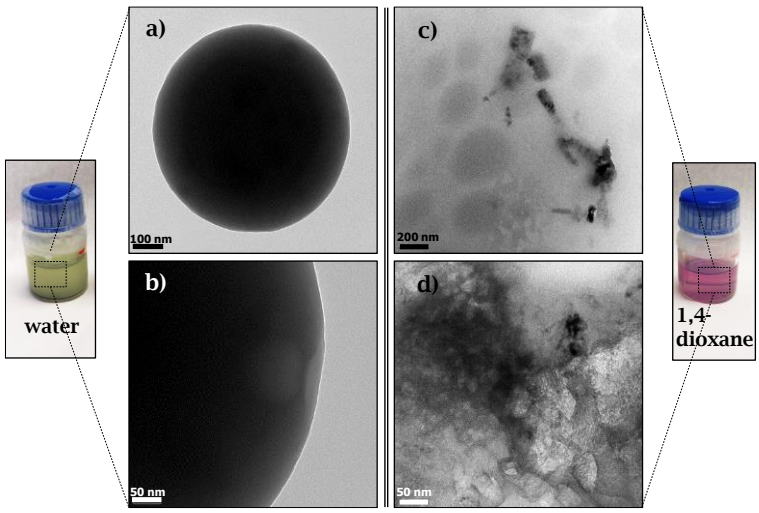

Fig. 10. Pictures of [Zn-(*R,R,R,R*)-**1**-(PS-*b*-P4VP)] solutions in water (greenish) and 1,4-dioxane (pink) and TEM images of: a) and b) [Zn-(*R,R,R,R*)-**1**-(PS-*b*-P4VP)] micelles in water and, c) and d) [Zn-(*R,R,R,R*)-**1**-(PS-*b*-P4VP)] mixed compound in 1,4-dioxane. (a scale bar indicates 100 nm; b scale bar indicates 50 nm; c scale bar indicates 200 nm; d scale bar indicates 50 nm)